NOTICE CONCERNING COPYRIGHT RESTRICTIONS

Thermal-Hydrodynamic-Chemical (THC) Model Calibration Study Based on Geothermal Field Data

Alexey Kiryukhin[1,2], Tianfu Xu[1], Karsten Pruess[1], John Apps[1], Igor Slovtsov[2]

[1]Earth Sciences Division, Lawrence Berkeley National Laboratory, MS90-1116, 1 Cyclotron Rd , Berkeley CA 94720, USA
[2]Institute of Volcanology, PIIP-9, Petropavlovsk-Kamchatsky, 683006, Russia

Keywords

Thermal, hydrodynamic, chemical, TOUGHREACT, geothermal fields

ABSTRACT

Available data on secondary mineral distributions, host rock properties, gas and the chemical compositions of geothermal fluids of geothermal fields in Kamchatka and Japan were used to calibrate thermo-hydrodynamic-chemical (THC) models using the TOUGHREACT numerical code (Xu and Pruess, 2001) [20,21]. The influence of thermodynamic and kinetic parameters of chemical interaction, and mass fluxes on mineral phase changes was found to be significant.

Introduction: Geothermal Fields Useful for THC Model Calibration

A number of geothermal fields associated with volcanic activity of the island arcs of the Kamchatka Peninsula and the Japanese islands are well described, and have thermal, hydrologic and geochemical features in common. They therefore lend themselves particularly to the testing of Thermo-Hydrodynamic-Chemical models (THC) in order to identify areas for model improvement, and for testing concepts relating to model calibration and validation. In this paper, we present preliminary results using the information of two Kamchatka and twelve Japanese geothermal fields currently found useful for THC model calibration (Figure 1, Tables 1 and 2). A brief description of these fields and pertinent references follow.

Mutnovsky [7,8]. High temperature liquid upwells from the south-east in a 80 m-thick fracture zone. A deep 280°C liquid-dominated zone shows quartz-epidote-chlorite secondary hydrothermal mineralization. Overlying this zone, ascending fluids encounter two-phase conditions characterized by prehnite-wairakite precipitation. Host rocks are diorites, Miocene-Pliocene sandstones, rhyolite, and andesitic tuffs and lavas.

Pauzhetsky [16]. Sub-lateral liquid flows at temperatures of 180-200°C occur within Pliocene-Quaternary welded rhyolitic and andesitic tuffs. The dominant secondary minerals are zeolites (mostly laumontite), carbonates and chlorites. Secondary K-feldspar (adularia) occurs in an upper high temperature zone, whereas secondary Na-feldspar (low-albite) is present in adjacent temperature inversion zones.

Nigorikawa (Mori) [6]. Host reservoir rocks are limestones intruded by andesite dikes. A Na-Cl-CO_2 enriched (8g/kg) liquid phase is present at 270°C.

Matsukawa [5]. The geothermal reservoir occupies dacite and rhyolite welded tuffs on the contact zone with a quartz diorite intrusion. Heat pipe conditions at pressures of 20-30 bars and temperatures of 200–240°C are observed. Pyrophyllite was found as the principal secondary mineral in production zones.

Sumikawa [1,19]. The reservoir consists mainly of Tertiary altered andesite, intruded by granite. The production zone occurs under two-phase conditions with temperatures up to 300°C, and is delineated by zeolites (wairakite), epidote and chlorite.

Kakkonda [12]. The reservoirs occupy Miocene andesitic and dacitic tuffs, and are liquid at temperatures from 220-260°C at shallow depth and 280-340°C at greater depth. They are delineated by epidote, anhydrite, sericite, prehnite and K-feldspar.

Uenotai [13,18]. The reservoir host rocks consist of Miocene andesite and pre-Tertiary granite. The central zone of the reservoir is boiling at 300°C. Production zones are delineated by secondary quartz, epidote, calcite and zeolites (wairakite).

Okuaizu [11,14]. The reservoir zone occurs along two faults within fractured Neogene "green tuff" formations (subaqueous tuffs and lava altered to a greenish color). High salinity and gas enriched geothermal fluid circulation is characterized by secondary calcite, anhydrite, chlorite and sericite occurrences at 250-300°C. A shallow reservoir is delineated by K-feldspar.

Hachijo-jima [10]. The high-temperature liquid dominated system exists in fractures in Tertiary andesite and basalt formations. Secondary minerals distributed in the upper part of the 300°C upflow region are: quartz, calcite and anhydrite. Production zones are characterized by wairakite.

Takigami [4]. Reservoir host rocks are andesitic and dacitic tuffs and lava in two fault/fracture systems. The parental liquid phase is at a temperature of 250°C and discharges laterally. The production reservoir is traced by the distribution of illite-chlorite. The locations of the upper limit of the zeolite minerals, laumontite and wairakite, coincide with the current temperature contours, at about 150 and 200°C, respectively.

Hatchubaru [3]. The host reservoir rocks include fractured pyroxene andesites transected by five main fault zones. The parental liquid is at 300°C. Hydrothermal alteration along ascending fluid flow includes a silicified zone of zeolites and feldspar (with anhydrite and calcite), an aluminosilicate zone, and an alunite zone.

Oguni [22]. The reservoir is composed of Quaternary dacitic pyroclastics and andesites. The parental liquid is at 240°C. Calcium carbonate scaling was observed under wellbore flashing conditions. Secondary mineralogy has not been described, but should be similar to that of the Pauzhetsky geothermal field.

Ogiri [2]. This field occurs within the single 20m wide Ginyu fault zone. The liquid reservoir is in andesitic host rocks at 232°C. Secondary quartz, wairakite, K-feldspar, chlorite and epidote are present in the production zone.

Fushime [15]. The main reservoir is composed of andesitic-dacitic lavas and tuffs in two fractured zones developed around a dacite intrusion. The liquid phase production zone is at 300°C and originated from CO_2 enriched heated sea water. The production zones are characterized by chlorite, epidote and K-feldspar, whereas Na-feldspar (albite) is found in the peripheral parts of the hydrothermal reservoir.

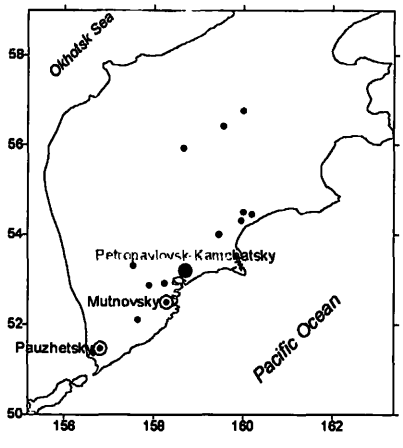

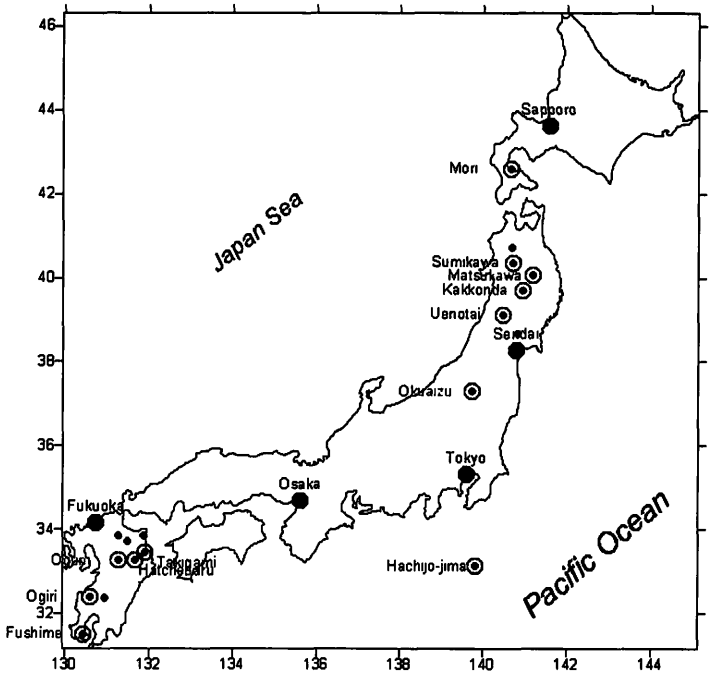

Figure 1. Geothermal fields of Kamchatka (Russia) and Japan, indicated by small circles. Those field currently found useful for THC studies are identified by double circles.

Model Setup (Liquid 260°C Upflow in Andesites, Ogiri Case)

Reservoir engineering study data of known geothermal fields shows that high temperature NaCl and CO_2 enriched *"parental geothermal fluids"* (Table 1) ascend through high-permeability zones, ("geothermal reservoirs"), and eventually discharge at the earth's surface. The principal contributors to secondary mineral precipitation in reservoirs under high temperatures conditions include quartz, wairakite, K-feldspar, chlorite, epidote, calcite, anhydrite, prehnite and sericite (Table 2). Based on the above information, a simplified streamline numerical model of a hydrothermal system may be expressed as a series of connected consecutive model elements B 1, R_1-R_n and D 1 (Figure 2). B 1 is a basement element, where the "parental geothermal fluid" originates. The R_n-elements, through which the "parental geothermal fluid" ascends, are at specified temperature steps. D 1 is a discharge element with assigned constant atmospheric pressure and surface temperature conditions. Temperatures in all elements are kept constant, and a steady state fluid flow through the system is specified. Using the above model, a test problem was designed to study the long-term chemical interaction of the "parental geothermal fluid", which is discharged through the model elements starting from B 1 under a specified range of temperatures. The rate law:

$$r = kS\,(1-Q/K)\,\exp(E_a/(R*298.15)-E_a/(RT))$$

where k is the chemical dissolution/precipitation kinetic rate constant at 25°C, mol/s m^2; S is specific reactive surface area, m^2/m^3; K is the equilibrium constant for mineral-water interaction; Q is the corresponding activity product; E_a is the activation energy of the reaction, kJ/kmol; R is the gas constant, kJ/mol K and T-temperature, K. The rate law is used for modeling kinetically controlled mineral dissolution and precipitation.

Hydrothermal upflow in andesites is very common: 93% of the host reservoir rocks in the studied geothermal fields are andesites, or include andesites as the principal host rock. A number of geothermal fields are liquid dominated at temperatures under 260°C, e.g. Ogiri, Takigami, Oguni, Pauzhetsky (Table 2). The Ogiri geothermal field was selected for model simulation and is typical of Kamchatka and Japanese fields. The geometry of the Ginyu fault zone, which is the production reservoir of the Ogiri geothermal field, is shown in Figures 3 and 4, overleaf. A mass flux of 2,500 kg/s km^2 is assumed in the model (Figure 2, overleaf) corresponding to Ginyu fault parameters and in the model are as follows: 20 m width, 700 m strike length, 35 kg/s natural fluid upflow rate (we assume that natural fluid upflow in Ginyu fault is about of 5 % of the total production, which is estimated at 700 kg/s [2]).

Because the current thermodynamic database is incomplete and restricted to end member phases in solid solution series,

Table 1. Gas and fluid chemistry data of Japanese and Kamchatka (Russia) geothermal fields (mg/kg) converted to deep reservoir conditions ("parental geothermal fluids"). Note: The enthalpy data is used for steam and separated water species normalization, pH correction is based on the approach by Reed and Spycher (1984) [17].

Geothermal Field, well	Enthalpy kJ/kg/ Tempera -ture,°C	pH 25	pH, cor.	Na	K	Ca	Mg	Fe	Al	Cl	SO_4	HCO_3	CO_3	As	B	SiO_2	CO_2	H_2S	H_2	R gas
Nigorikawa	1150 270			3,900						6,100							8,000			
Matsukawa, M-3	2800 250																12,580	1,090		275
Sumikawa, SC1	1560 300	7.6	7.3	322	54.0	5.2	1.3	0.1	0.1	265	47.6	24.6		7.5	123.8	665	138	79	0.1	240
Kakkonda, 19	1450 340	4.0	4.2	412	93.6	10.9	0.3	11.5	0.5	762	34.3			2.5	17.6	811	249	46	1	23
Uenotai, T-45	1692 300	9.5	7.6	94	19	0.2	0.0			122	1.1			0.1		412	1,541	198	2.8	38
Okuaizu, 87N-15T	1500 300		6.6	5,202	1,451	769	7.0	1.2	0.5	11,100	5					733	51,323	1,429	0	159
Hachijo-jima,HT-1	2650 300	6.2	5.3	110	6.2	13.5	0.1			191	6.4	0.2					14,928	1,190	19	22
Takigami, TT14	1025 250	9.1	8.0	385	68.2	6.4	0.1			602	73		41		7.5	455	446	46		16
Hatchubaru, H-17	1100 300	8.0	4.7	860	120	32	0.1			1,430	96				23	510	8,670	200		70
Oguni, OH20	1180 240	8.8	7.4	689	97.2	16	0.01	0.01	0.6	1,175	42.1	41.3			15.1	446	269	5.6		8
Ogiri, NT-A1	963 232	8.7	7.7	335	40.6	8.4	0.01		0.9	453	150.4	12.2		0.0	29.5	477	31	1.8		
Fushime, 19	1998 300	5.8	5.2	3,628	1,095	402	1.9			7,872	22.7				27.2	319	2,181	432	2	22
Mutnovsky, 029W	1200 300	7.9	6.9	157	29.6	1.3	0.0			185	80.3	53.9				683	2,140	435	2	
Pauzhetsky, 106	820 220	8.5	7.4	595	47.3	39.6	0.0			1,139	102	9.4		2.5	19.5	199	6			11

Table 2. Principal secondary minerals in the production reservoirs of the geothermal fields.

Geothermal Field	Base Temperature oC and Phase Conditions	Production Reservoir Host Rocks	Principal Secondary Hydrothermal Minerals Occurence													
			Quartz	K-feldspar	Na-feldspar	Wairakite	Laumontite	Calcite	Anhydrite	Chlorite	Illite	Smectites	Epidote	Prehnite	Sericite	Kaolinite
Mori (Nigorikawa)	270 Liquid	Limestones, andesites						⊕								
Matsukawa	250 Steam	Dacite and rhyolite welded tuffs												⊕		
Sumikawa	300 2-phase	Andesites and granites.				⊕				⊕			⊕			
Kakkonda	340 Liquid	Andesitic and dacitic tuffs	⊕	⊕					⊕				⊕	⊕	⊕	
Uenotai	300 2-Phase Liquid	Andesites and granite	⊕			⊕		⊕					⊕			
Okuaizu	300 Liquid	Rhyolite and andesite tuffs.		⊕				⊕	⊕	⊕					⊕	
Hachijo-jima	300 Liquid	Andesites and basalts	⊕			⊕		⊕	⊕							
Takigami	250 Liquid	Andesitic and dacitic tuffs and lavas				⊕	⊕			⊕	⊕					
Hatchubaru	300 Liquid	Pyroxene andesites		⊕			⊕	⊕	⊕							
Oguni	240 Liquid	Dacitic tuffs and andesites						⊕								
Ogiri	232 Liquid	Pyroxene andesites	⊕	⊕		⊕				⊕			⊕			
Fushime	300 Liquid	Andesitic-dacitic lavas and tuffs		⊕	⊕					⊕			⊕			
Mutnovsky	300 Liquid, 2-Phase	Diorites, sandstones, rhyolite, andesite tuffs and lavas	⊕			⊕				⊕			⊕	⊕		
Pauzhetsky	220 Liquid	Welded rhyolite tuffs,andesite tuffs and lavas	⊕	⊕			⊕	⊕		⊕						

several proxy minerals that in aggregate reflect the bulk chemical composition of this host rock were chosen to represent the actual mineral composition of an unaltered pyroxene andesite. The initial mineral composition of the reservoir is therefore represented: 45% anorthite (Ca-feldspar), 26% albite-high (Na-feldspar), 11% sanidine (K-feldspar), 16% diopside, 2% quartz. Fortunately, the impact of these necessary substitutions on the described model simulations is minor, because all primary proxy minerals except quartz are unstable with respect to the secondary minerals. Total porosity was assigned a value of 0.1. The kinetic parameters of chemical interaction are given in Table 3. The "parental geothermal fluid" with a chemical composition

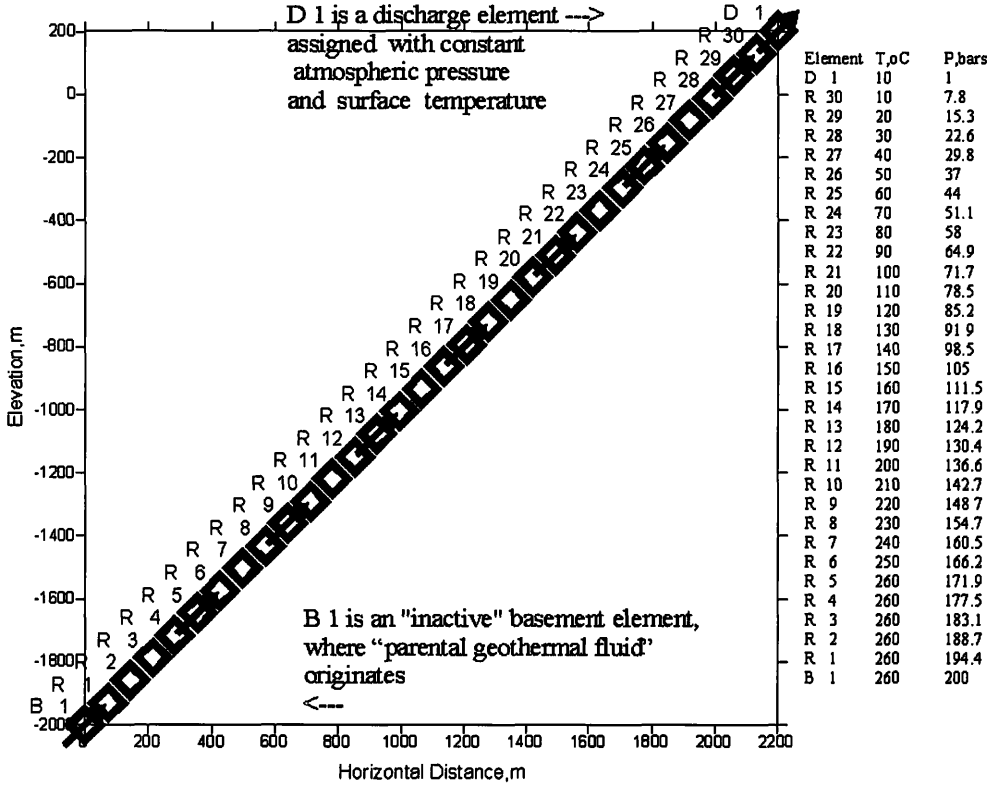

Figure 2. Streamline model of ascending parental geothermal fluid flow in a geothermal reservoir including the numerical grid, initial and boundary conditions used in the model.

Table 3. Kinetic parameters for chemical interaction (k - chemical dissolution / precipitation kinetic rate constant at 25°C, mol/s m²; S - surface area, m²/m³; and E_a-activation energy, kJ/kmol). Notes: k and E_a values: quartz, feldspars, chlorite, illite, smectites, and kaolinite from [20], cristobalite, opal, amorphous silica, zeolites (wairakite, laumontite, mordenite) from E. Sonnenthal (pers. com., 2002), diopside kinetic parameters are set to those of the feldspars. S values are calibrated in the model.

Minerals	Formulae	k mol/s m²	S m²/m³	E_a kJ/mol
Calcite	$CaCO_3$	Minerals		
Anhydrite	$CaSO_4$	at equilibrium		
Quartz	SiO_2	4.3e-14	1.0e+3	75.0
Microcline(K-feldspar)	$K\ AlSi_3O_8$	1.0e-12	1.1e-3	67.83
Albite-high(Na-feldspar)	$Na\ AlSi_3O_8$	1.0e-12	2.6e-4	67.83
Albite-low (Na-feldspar)	$Na\ AlSi_3O_8$	1.0e-12	1.0e-4	67.83
Anorthite(Ca-feldspar)	$Ca\ Al_2Si_2O_8$	1.0e-12	4.5e-2	67.83
Diopside	$CaMgSi_2O_6$	1.0e-12	1.8e-1	67.83
Cristobalite-a	SiO_2	3.4491e-13	1.0e+3	68.9
Opal	SiO_2	3.4491e-13	1.0e+3	68.9
Amorphous Silica	SiO_2	7.3234e-13	1.0e+3	62.9
Wairakite	$Ca[Al_2Si_4O_{12}]\ 2H_2O$	2.5e-13	1.0e+2	58.0
Laumontite	$Ca[Al_2Si_4O_{12}]\ 4H_2O$	2.5e-13	1.0e-2	58.0
Mordenite	$(Na_2,K_2,Ca)[Al_2Si_{10}O_{24}]\ 7H_2O$	2.5e-13	1.0e-1	58.0
Illite	$K\ Al_4[Si_7AlO_{20}](OH)_4$	1.0e-14	1.0e-1	58.62
Ca-Smectite	$Ca_{0.3}Al_{3.5}Mg_{0.5}(Si_8O_{20})(OH)_4$	1.0e-14	1.0e-3	58.62
Mg-Smectite	$MgAl_{3.5}(Si_8O_{20})(OH)_4$	1.0e-14	1.0e-3	58.62
Na-Smectite	$Na_{0.6}Al_{3.5}Mg_{0.5}(Si_8O_{20})(OH)_4$	1.0e-14	1.0e-3	58.62
Chlorite	$Mg_{10}Al_2[Si_6Al_2O_{20}](OH)_{16}$	1.0e-14	1.0e+1	58.62
Kaolinite	$Al_4[Si_4O_{10}](OH)_8$	1.0e-13	1.0e-1	62.76

corresponding to that of the Ogiri geothermal field (Table 1) was injected into the model geothermal reservoirs (Figure 2). The following secondary hydrothermal minerals are included in the system (in addition to the source minerals mentioned above): calcite, anhydrite, albite-low, wairakite, laumontite, mordenite, Na, Ca and Mg-smectites, chlorite, illite, amorphous silica, cristobalite, opal, kaolinite and prehnite.

Results

No Flow Scenario

Figure 5 shows the modeling scenario, where No Flow conditions are specified. In this case, replacement of high-albite by low-albite, significant precipitation of wairakite (0.0032 volume fraction at 240°C) and laumontite, and dissolution of anorthite and quartz was observed after 1,000 years, which can be represented by the reaction:

$$CaAl_2Si_2O_8 + 2SiO_2 + 2H_2O \rightarrow CaAl_2Si_4O_{12} * 2H_2O$$

$$\text{Anorthite} + 2\ \text{Quartz} + 2H_2O \rightarrow \text{Wairakite}$$

This process is sensitive to rock porosity. If the porosity value is reduced below 0.001, then no significant zeolite formation would occur because of the limited availability of water in the residual pore space.

Mass Flux Scenario

Figure 6 shows the mineral phase distribution for the modeling scenario, where "Mass Flux" conditions are specified. In this case, the SiO_2 and K/Na enriched "parental geothermal fluid" mass flux is superimposed, which induces SiO_2 precipitation and Na-K feldspar exchange reactions, causing significant quartz and K-feldspar accumulation. The relatively K^+ enriched inflow through the system serves as a source of K for K-feldspar precipitation, thus:

$$NaAlSi_3O_8 + K^+ \rightarrow KAlSi_3O_8 + Na^+$$

$$\text{Na-feldspar (Albite)} + K^+ \rightarrow \text{K-feldspar (Microcline)} + Na^+$$

The replacement of high-albite by low-albite, precipitation of wairakite (0.0025 volume frac-

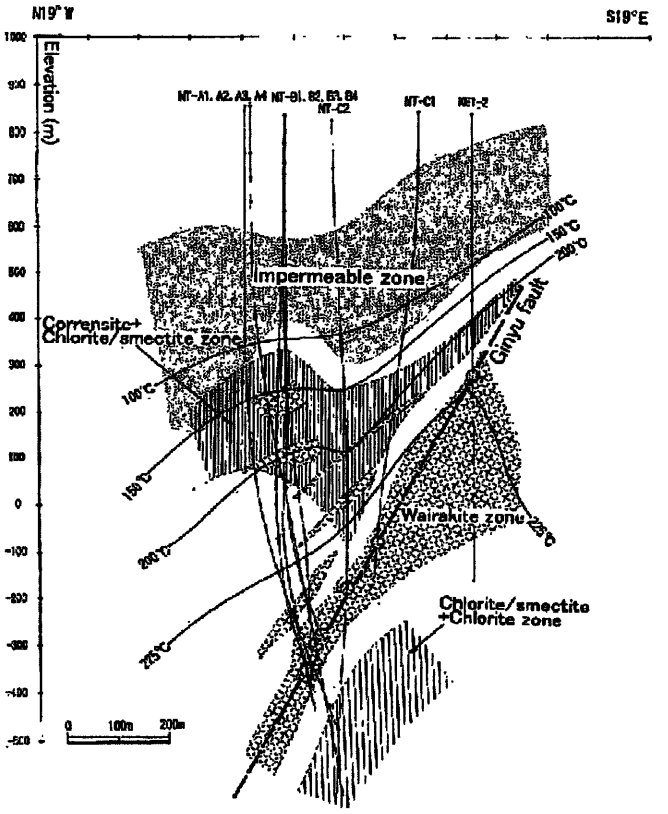

Figure 3. A cross section showing the distribution of clay minerals and wairakite around the Ginyu fault zone. All wells are projected onto the section perpendicular to the plane of the Ginyu fault. Open circles represent the Ginyu fault intersections in the production wells [2].

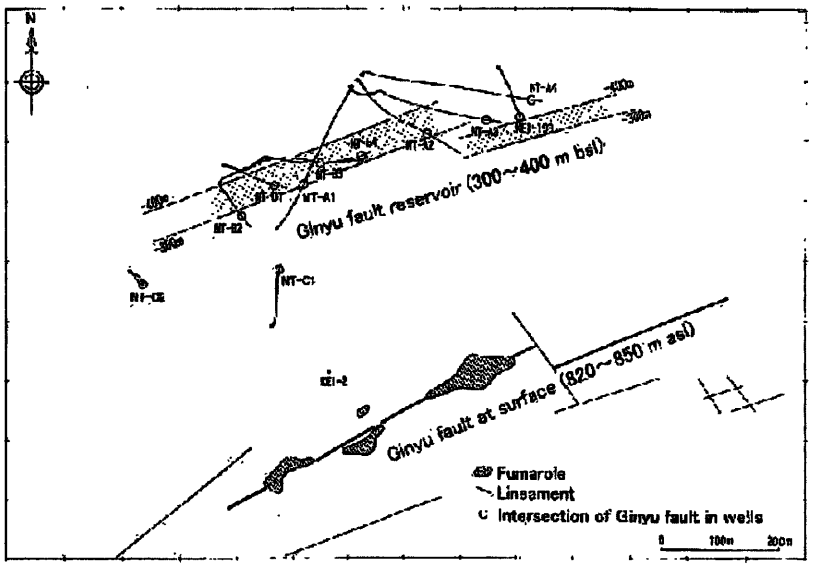

Figure 4. Surface trace and subsurface projection of the Ginyu fault. Solid circles - well location at the surface; asl - above sea level; bsl - below sea level [2].

tion at 240°C) and laumontite, and dissolution of the source minerals: anorthite and diopside is also observed after 1,000 years. A significant amount of chlorite, illite, smectite and kaolinite is also precipitated.

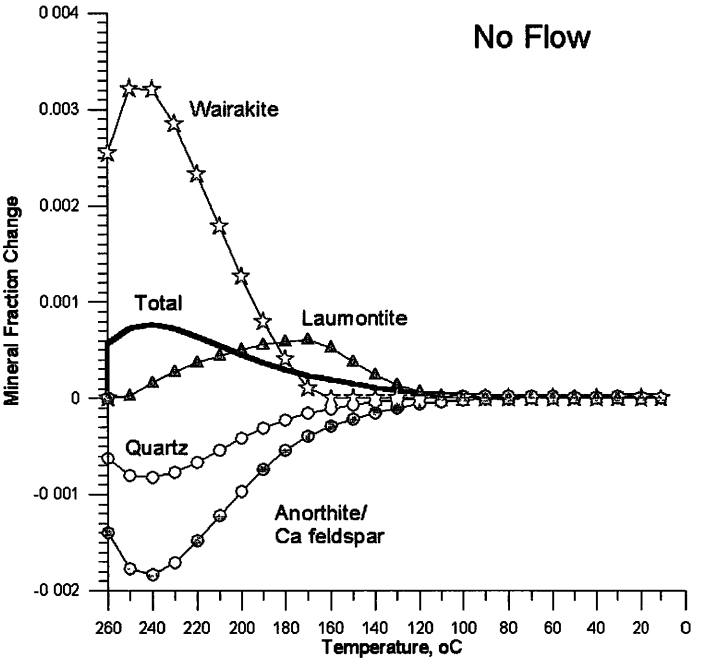

Figure 5. Change in volume fraction of the mineral phases along model reservoir after 1,000 years under "No Flow" conditions.

Discussion of Modeling Results

(1) ***Model/field data match.*** Wairakite, quartz, K-feldspar and chlorite precipitates obtained in the model as the principal secondary minerals in the production zone, and the illite-smectite maximum at 200°C, matches observations in the Ogiri geothermal field. A core sample from the upper part of Ginyu fault (well KE1-2) shows a 1740 mm vein filled by wairakite and quartz at 222°C [2]. Secondary K-feldspar was also detected in the Ginyu fault (well NT-A1)[2]. Drilling observations show that the presence of chlorite-smectite indicates a proximity to the Ginyu fault, and whether or not a well has been drilled completely through the fault zone [2].

(2) The *calibration procedure* includes adjustment of the mineral surface areas (Table 3) and removing inappropriate secondary minerals to match model and geothermal field data (Table 2). While the surface areas of quartz and silica product minerals are relatively high, other mineral areas were reduced significantly (feldspars and smectites especially). Otherwise quartz precipitation will not occur in quantities consistent with field observation. One possible explanation is that Ca-Na-K feldspars in andesites are in solid solution, which restricts surface area compared to simple mixtures of feldspars end members. Clays (smectites) are supersaturated along all ascending upflow zones, but were "prohibited" in the model from precipitating significantly by reducing the surface area.

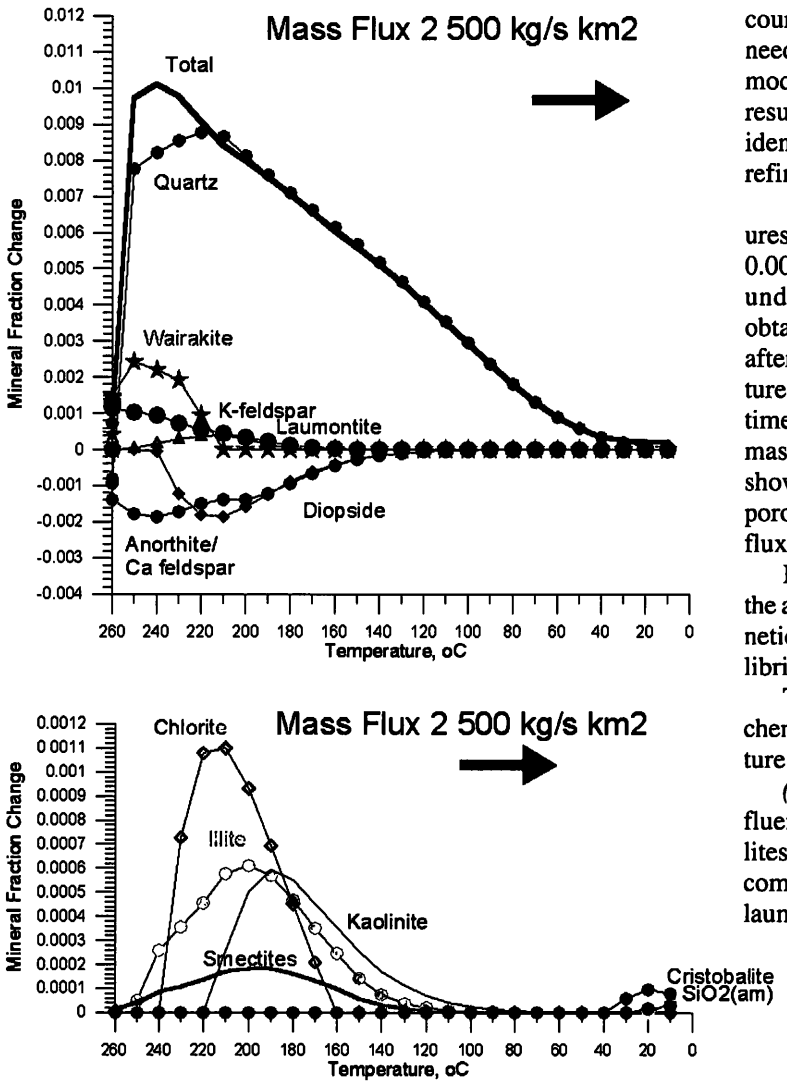

Figure 6. Change in volume fraction of mineral phases along the ascending flow path (Mass Flux conditions) after 1,000 years. Upper graph – principal mineral phases, lower graph – minor secondary mineral phases.

Prehnite was eliminated from the system because the thermodynamic properties are suspect. The introduction of sericite in the geochemical system might probably overcome the problems associated with preferential precipitation of prehnite.

The above described calibration procedure is somewhat arbitrary, and reflects the current uncertainties in adequately defining both mineral dissolution kinetics and the uncertainties in specifying mineral reactive surface areas in the model. Furthermore, the current algorithm describing heterogeneous reaction kinetics does not adequately reflect geochemical processes consistent with the so-called Ostwald Rule of Stages. For example, polymorphs with identical mineral stoichiometries, e.g., the silica polymorphs, precipitate simultaneously; a process that is effectively prohibited by the rule. Similar arguments might likewise be advanced with respect to the relative appearance and stability of wairakite and laumontite in geothermal systems (see below). These issues and others recognized during the course of the evaluation presented in this paper, highlight the need for a more sophisticated approach to reactive transport modeling than has hitherto been considered. Nevertheless, the results presented here are encouraging, and form the basis for identifying those issues that require further attention in future refinements to the THC modeling of geothermal processes.

(3) ***Significant porosity reduction*** caused by flow (Figures 5, 6). Under no-flow conditions, a porosity reduction of 0.0008 (partially through zeolite precipitation) occurs, while under flowing conditions a 0.0100 porosity reduction is obtained(by quartz, zeolites, and additionally by K-feldspar) after 1,000 years. It was found also that the 0.10-porosity fractures will be completely sealed after 5,000 years of modeling time at a mass flux 2,500 kg/s km^2. A porosity reduction vs. mass flux change in the range of (0 to 250,000 kg/s km^2) is shown in Figure 7. It follows from Figure 7 that the same 0.10-porosity fractures will be 80% sealed after 100 years, if the mass flux is increased from 2,500 to 250,000 kg/s km^2.

Na/K fluid temperature buffer (log(Na/K)=f(T)) is based on the albite/microcline equilibrium under saturated conditions. Kinetic effects may displace the activity coefficients from equilibrium at temperatures under 200°C, as shown above.

The following discussion is a brief interpretation of the key chemical interactions, which cause porosity reduction in the fracture system.

(a) Zeolites. Mass flux conditions do not significantly influence the temperature dependence on the production of zeolites (wairakite at 220-260°C, and laumontite at 180-240°C) compared to "no flow" conditions (wairakite 180-260°C, and laumontite 140-240°C). All necessary chemical components for zeolites are available in the water saturated andesites (if the porosity value is over 0.001), as discussed above.

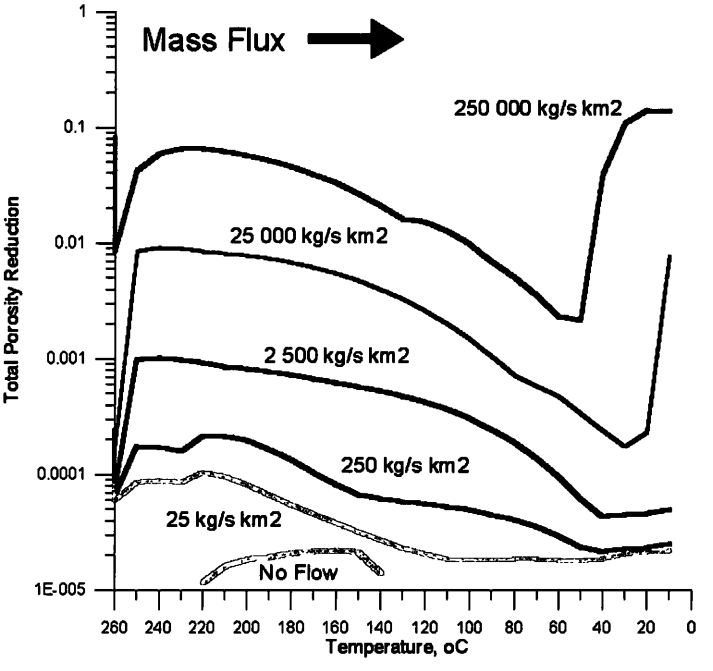

Figure 7. Porosity reduction along ascending flow path at different mass fluxes (0 – 250,000 kg/s km2) after 100 years.

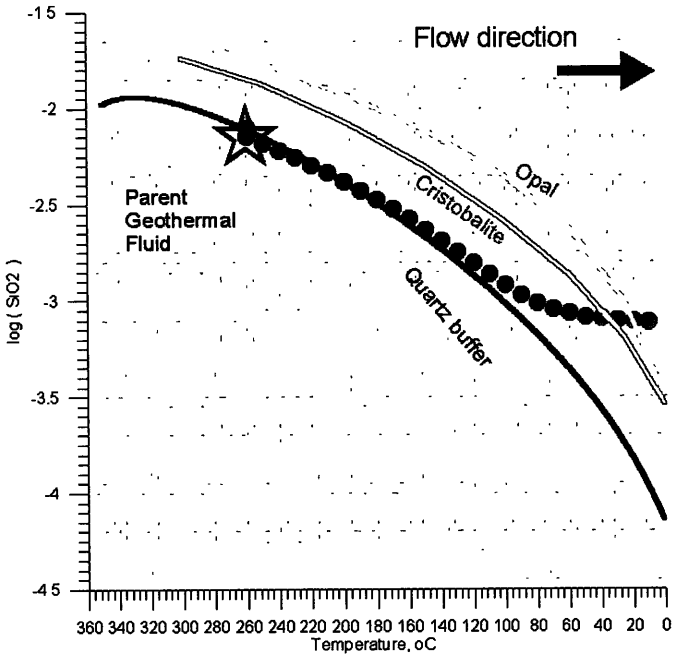

Figure 8. Distribution of log(SiO_2) along the ascending flow path after 1,000 years. SiO_2 fluid temperature buffer (log(SiO_2)=f(T)) is based on quartz equilibrium under saturated conditions. Kinetic effects may displace the concentration from equilibrium at low temperatures (under 120°C), as shown above.

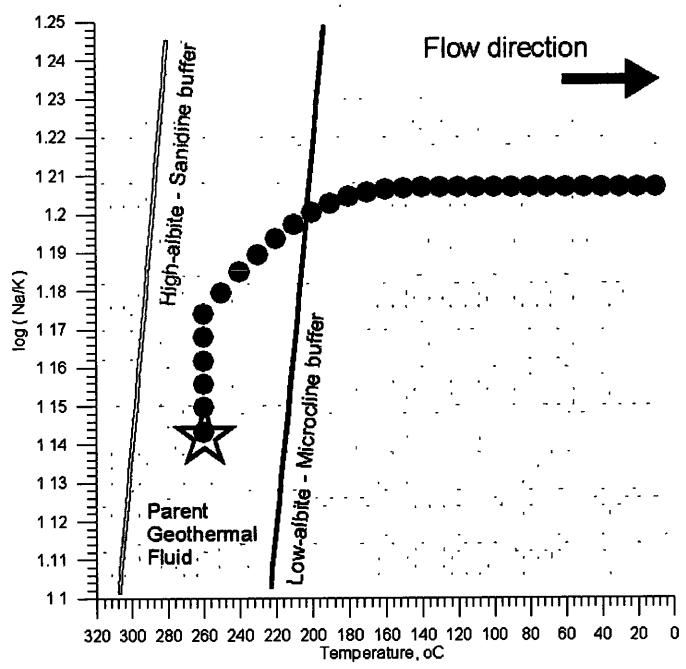

Figure 9. Distribution of log(Na/K) along the ascending flow path after 1,000 years.

Some extension of the laumontite temperature range is caused by additional water inflow into the system (laumontite needs an additional two moles of H_2O, compared to wairakite).

(b) Quartz and K-feldspar. Basically the precipitation of these minerals is a consequence of SiO_2 and Na/K fluid temperature equilibrium buffering under up-flow conditions (K^+ and SiO_2 from parental geothermal fluid), as alluded to earlier [9]. Figures 8 and 9 show how these buffers work in this specific case. The SiO_2 buffer is effective from 260°C to 120°C, before quartz supersaturation (Figure 8). The Na/K buffer is active between the albite-high and albite-low curves from 260°C to 200°C, before K-feldspar supersaturation occurs (Figure 9). Quartz and K-feldspar supersaturation at low temperatures are kinetically controlled.

(4) *Wairakite-laumontite thermodynamic problem.* The lower temperature limits of wairakite-laumontite precipitation obtained in the model are 220/180°C. This is a reasonable match to the Takigami geothermal field (200/150°C) [4] and Pauzhetsky geothermal field (max temperature 220°C) [16], where mostly laumontite was reported. In contrast, only wairakite was reported in the Ginyu fault production zone at Ogiri [2], although a similar range of temperatures, fluid chemistry and host rock composition is present. A possible explanation is the small difference in wairakite/ laumontite thermodynamic properties in range of temperatures 200-250°C, which make their occurrence very sensitive to small changes in source rock and fluid chemistry, and kinetic rate constants (Figure 10).

Conclusions

(1) Available data on secondary mineral distributions, host rock properties and chemical compositions of parental geothermal fluids of the geothermal fields Kamchatka and Japan have been used for the calibration of a THC model. In particular, THC modeling of the liquid upflow at 260°C in andesites, represented by the Ogiri, Japan, geothermal field, was selected as representative. Wairakite, quartz, K-feldspar and chlorite formed in the model as the principal secondary minerals in the produc

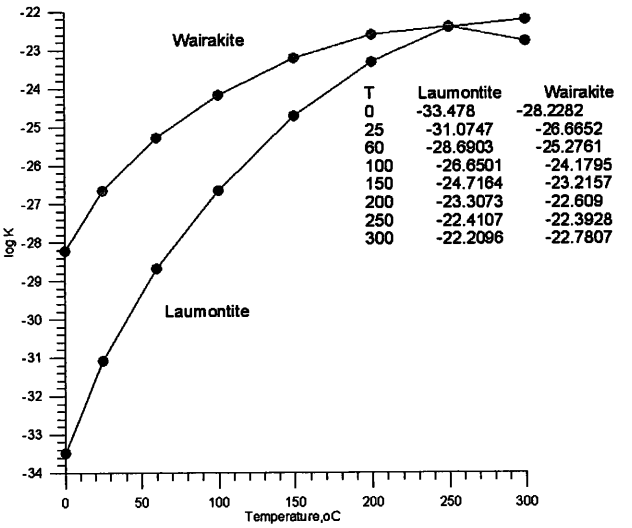

Figure 10. Wairakite and laumontite equilibrium constants (log K) vs. temperature. Note, that difference in log K between wairakite and laumontite of 230°C (503°K) is only 0.4, equivalent to 0.4 RT 2.303 = 3.8 kJ/mol, which is within the uncertainty of the thermodynamic data used in the simulation.

tion zone, and illite-smectite formed below 230°C. These results match observations in the Ogiri geothermal field.

(2) THC modeling shows a significant influence of thermodynamic and kinetic parameters of chemical interaction, and mass flux on mineral phase formation along the ascending flow path. It was found that no parental geothermal fluid inflow is needed for zeolite precipitation, which occurs above 140°C in saturated andesite (if the porosity is greater 0.001). In contrast, quartz and K-feldspar precipitation may result in a significant porosity reduction over a thousand year time scale under mass flux conditions (complete fracture sealing will occur given sufficient time).

(3) Further development of the THC model of active hydrothermal systems is required and includes refinements to the thermodynamic and kinetic databases, and the development of more sophisticated algorithms describing heterogeneous reaction kinetics. The application of the model to other geothermal fields is also needed to provide a basis for model validation.

Acknowledgements

The authors express their gratitude for helpful discussion to G. Bodvarsson, A. Simmons, A. Truesdell, R. Fournier, M. Reed, N. Spycher, S. Fedotov,V. Belousov, S. Flexser, M. Lippmann, E. Sonnenthal, K. Williamson, P. Kruger, P. Dobson, M. Hanano, T. Shimoike, E. Lima, M. Momita, N. Tsuchiya, L. Richard, S. Salah and E. Kalacheva.

This work was supported by the Assistant Secretary for Energy Efficiency and Renewable Energy, Office of Power Technologies, Office of Wind and Geothermal Technologies, of the U.S. Department of Energy under contract No. DE-AC03-76SF00098.

References

1. K.Ariki, H.Kato, A.Ueda, M.Bamba (2000) Characteristics and Management of the Sumikawa Geothermal Reservoir, Northeastern Japan. Geothermics, v.29, p.171-189.

2. K.Goko (2000) Structure and hydrology of the Ogiri field, West Kirishima geothermal area , Kyushu , Japan // Geothermics, v.29, N.2, p.127-149.

3. S. Furuya, M. Aokia, H. Gotoha,T. Takenaka (2000) Takigami geothermal system, northeastern Kyushu, Japan Geothermics 29 p.191-211.

4. T.Fujino, T.Yamasaki (1984) Geologic and Geothermal Structure of the Hatchubaru Field, Central Kyushu, Japan. Geothermal Resources Council, Transactions, Vol.8, p.425-430.

5. Hanano M., and Matsuo G. (1990) Initial State of the Matsukawa Geothermal Reservoir: Reconstruction of a Reservoir Pressure Profile and its Implications. Geothermics,v.19,pp.541-560.

6. Higo M. (1985) Geothermal country update of Japan. Proc. of International Symposium on Geothermal Energy, Hawaii, p.119-134.

7. Kiryukhin A.V. (1993) High temperature fluid flows in the Mutnovsky hydrothermal system, Kamchatka. Geothermics,v.23,N 1, p.49-64.

8. Kiryukhin A.V. (1996) Modeling Studies: the Dachny Geothermal Reservoir, Kamchatka, Russia. Geothermics, Vol.25, No.1, p.63-90.

9. A.Kiryukhin, T.Xu, Karsten Pruess, Igor Slovtsov (2002) Modeling of Thermo-Hydrodynamic-Chemical Processes: Some Applications to Active Hydrothermal Systems. 27-th Stanford Workshop on Geothermal Reservoir Engineering.

10. K.Matsuyama, N. Narita, K. Tomita, T. Majima (2000) // Geothermal resources of Hachijojima. Geothermics v.29, p.213-232

11. K.Mizugaki (2000) Geologic structure and volcanic history of the Yanaizu-Nishiyama (Okuaizu) geothermal field, Northeast Japan // Geothermics 29, p.233-256.

12. H. Muraoka, T. Uchida, M. Sasada, M. Yagi, K. Akaku, M. Sasaki, K. Yasukawa, S. Miyazaki, N. Doi, S. Saito, K. Sato, S. Tanaka (1998) Deep Geothermal Resources Survey Program: Igneous, Metamorphic and Hydrothermal Processes in a Well Encountering 500 °C at 3729 m Depth, Kakkonda, Japan. Geothermics Vol. 27, No. 5/6, pp. 507-534.

13. Naka T., Okada H. (1992) Exploration and development of Uenotai geothermal field, Akita prefecture, northeastern Japan. Resource Geology 42, 223-240 (in Japanese with English abstract).

14. Nitta T., Tsukagoshi S., Adachi M., Seo K. (1995) Exploration and development in the Okuaizu geothermal field Japan (In Japanese with English abstract), Resource Geol. 45, 201-212.

15. H.Okada, Y. Yasuda, M. Yagi, K. Kai (2000) Geology and fluid chemistry of the Fushime geothermal field, Kyushu, Japan. Geothermics 29, 279-311.

16. Pauzhetka Thermal Waters in Kamchatka (1965). Moscow, Nauka Publ., 205 p.

17. M.Reed and N.Spycher (1984) Calculation of pH and Mineral Equilibria in Hydrothermal Waters with Application to Geothermometry and Studies of Boiling and Dilution. Geochimica et Cosmochimica Acta, Vol.48, pp.1479-1492.

18. N. Takeno (2000) Thermal and geochemical structure of the Uenotai geothermal system, Japan. Geothermics 29, p.257- 277.

19. Ueda A., Kubota Y., Katoh H., Hatakeyama K., Matsubaya O. (1991) Geochemical characteristics of the Sumikawa geothermal system, northeast Japan. Geochemical Journal 25, 223-244.

20. T.Xu and K.Pruess (2001a) On Fluid Flow and Mineral Alteration in Fractured Caprock of Magmatic Hydrothermal Systems// Journal of Geophysical Research, Vol.106, No.B2, p.2121-2138.

21. Xu, T. and K. Pruess (2001b). Modeling Multiphase Non-Isothermal Fluid Flow and Reactive Geochemical Transport in Variably Saturated Fractured Rocks: 1. Methodology, American Journal of Science, Vol. 301, pp. 16-33.

22. M. Yamada, K. Iguchi, S. Nakanishi, N. Todaka (2000) Reservoir characteristics and development plan of the Oguni geothermal field, Kyushu, Japan Geothermics 29, p.151-169.